# Supplementary Information

## Supplementary Figures

Supplementary Figure 15: Scatter plots depicting non-fucosylated and fucosylated Gal3Man3GlcNAc6 levels in hormone-sensitive (n = 120), hormonally treated (n = 37), and hormone resistant (n = 75) tumor regions

Supplementary Figure 16: Significant N-glycans with a high degree of quantitative change in NE tumor regions

**Supplementary Datasets** (All supplementary datasets supplied as individual Excel files)

Supplementary Data 1: N-Glycan Mass Spectrometric Data Comparing N-Glycan Abundance Between Well-Differentiated and Poorly Differentiated Tumor Regions

Supplementary Data 2: N-Glycan Mass Spectrometric Data Comparing N-Glycan Abundance Between Well-Differentiated and Poorly Differentiated Tumor Regions for Patient 1

Supplementary Data 3: N-Glycan Mass Spectrometric Data Comparing N-Glycan Abundance Between Well-Differentiated and Poorly Differentiated Tumor Regions for Patient 2

Supplementary Data 4: N-Glycan Mass Spectrometric Data Comparing N-Glycan Abundance Between Well-Differentiated and Poorly Differentiated Tumor Regions for Patient 3

Supplementary Data 5: N-Glycan Mass Spectrometric Data Comparing N-Glycan Abundance Between Well-Differentiated and Poorly Differentiated Tumor Regions for Patient 4

Supplementary Data 6: N-Glycan Mass Spectrometric Data Comparing N-Glycan Abundance Between Hormone-Sensitive and Hormonally-Treated Tumor Regions

Supplementary Data 7: N-Glycan Mass Spectrometric Data Comparing N-Glycan Abundance Between Hormonally-Treated and Hormone-Resistant Tumor Regions

Supplementary Data 8: N-Glycan Mass Spectrometric Data Comparing N-Glycan Abundance Between Neuroendocrine and Mixed Adenocarcinoma Tumor Regions

Supplementary Data 9: N-Glycan Mass Spectrometric Data Comparing N-Glycan Abundance Between Neuroendocrine and Mixed Adenocarcinoma Tumor Regions in Patient 1

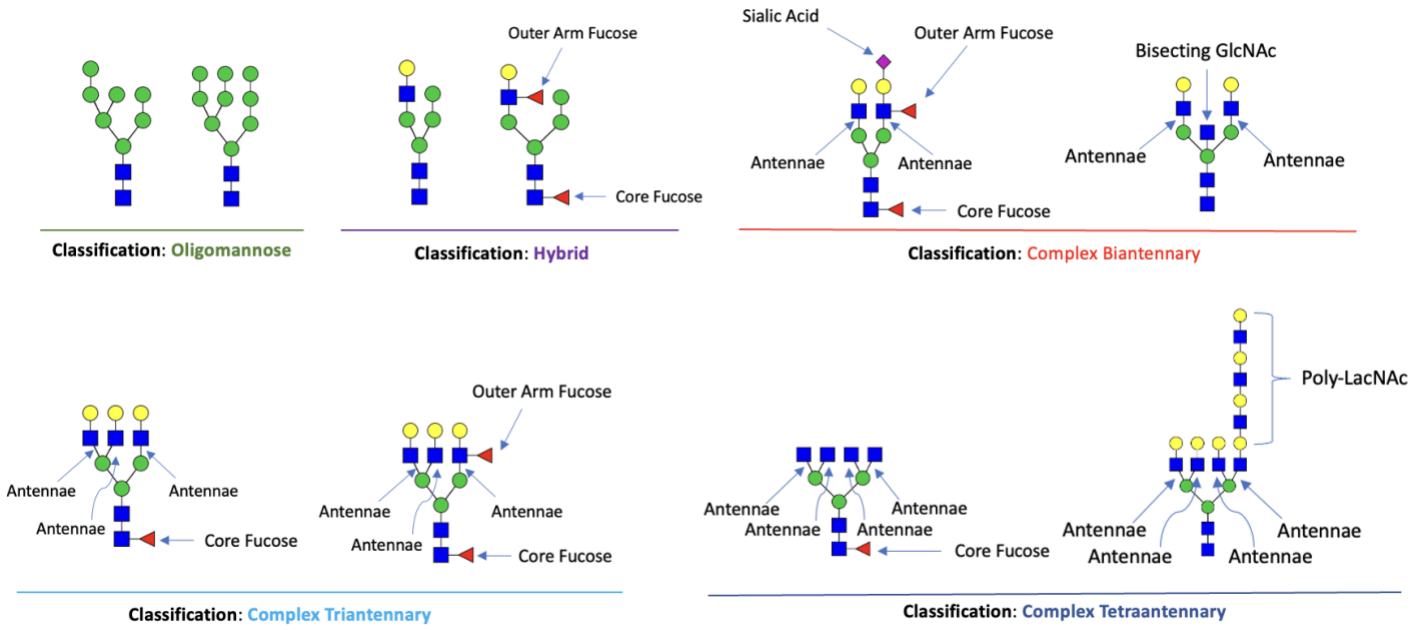


**Supplementary Figure 1. Summary of the major classes of N-glycans and common structural modifications**

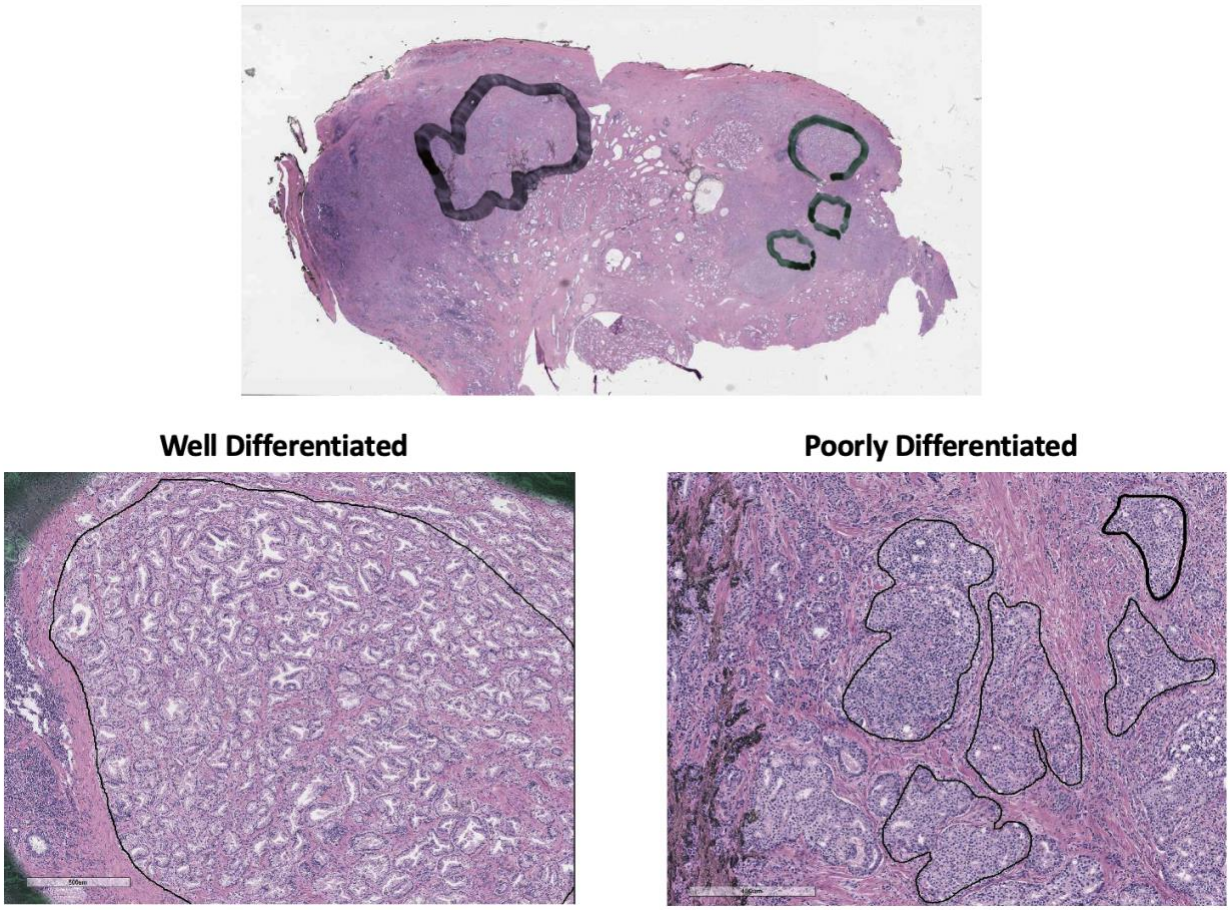


**Supplementary Figure 2**: **Representative H&E images of a patient case with both well-differentiated and poorly differentiated tumor cells on same FFPE slide. Upper panel demonstrates pathological annotation of targeted tumor regions (green = abundance of low grade tumor cells, black = abundance of high grade tumor cells). Lower panel demonstrates representative demarcated pure tumor cell regions within targeted areas.**

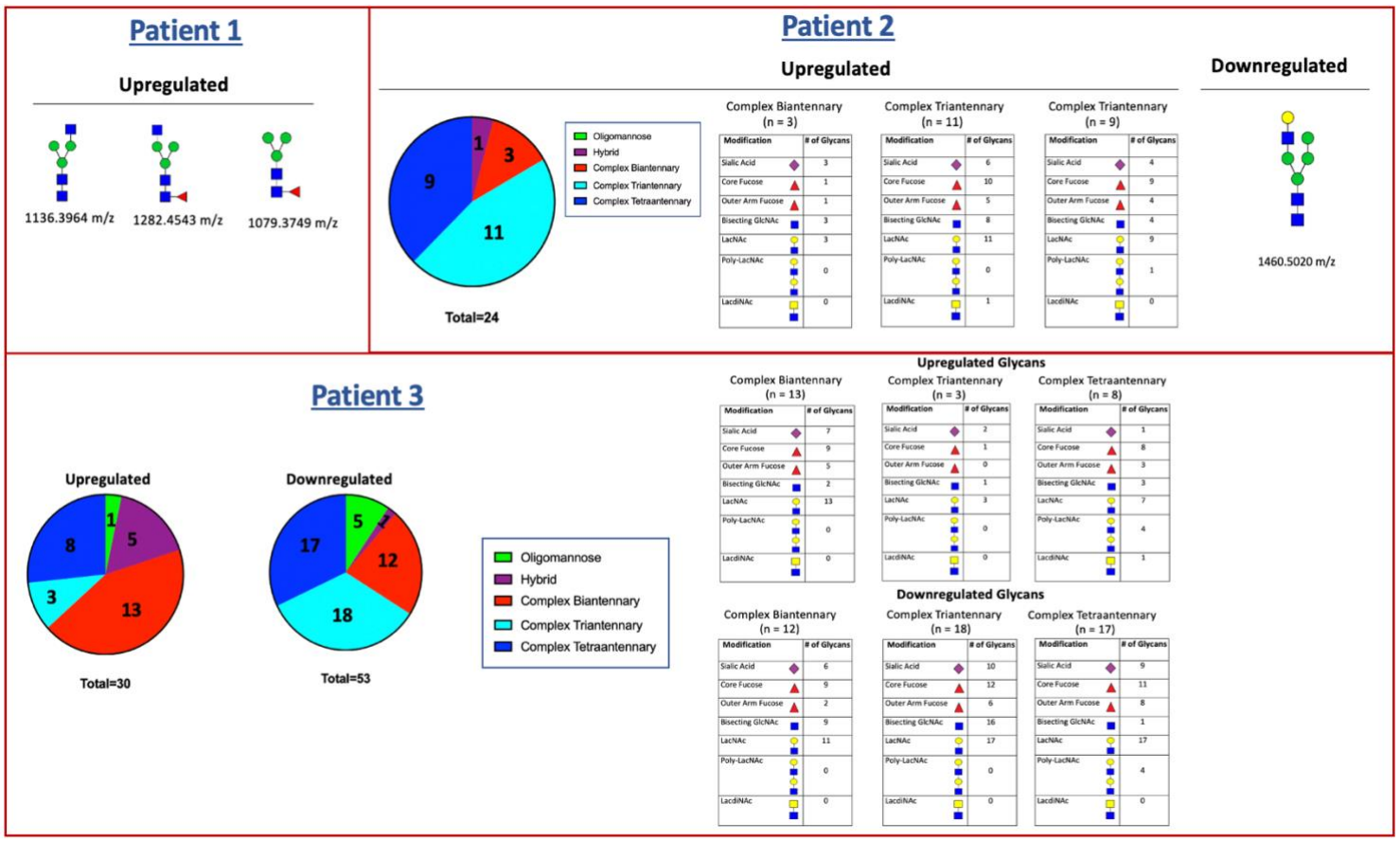


**Supplementary Figure 3: Analysis of N-glycosylation changes between well differentiated and poorly differentiated glands within each patient.** (Upper Left) Patient 1 demonstrates upregulation of 2 hybrid N-glycans (1136.3964 m/z and 1282.4543 m/z) and a core-fucosylated paucimannose structure (1079.3749 m/z) in poorly differentiated tumor regions (Upper Right) Patient 2 demonstrates upregulation of 24 structures and downregulation of 1 structure (1460.5020 m/z) in poorly differentiated tumor regions. The largest proportion of upregulated structures are complex tri- and tetraantennary forms. (Bottom) Patient 3 demonstrates upregulation of 30 structures and downregulation of 53 structures in poorly-differentiated tumor regions.. The largest proportion of upregulated structures were complex biantennary structures while the largest proportion of downregulated structures were complex tri- and tetraantennary forms.

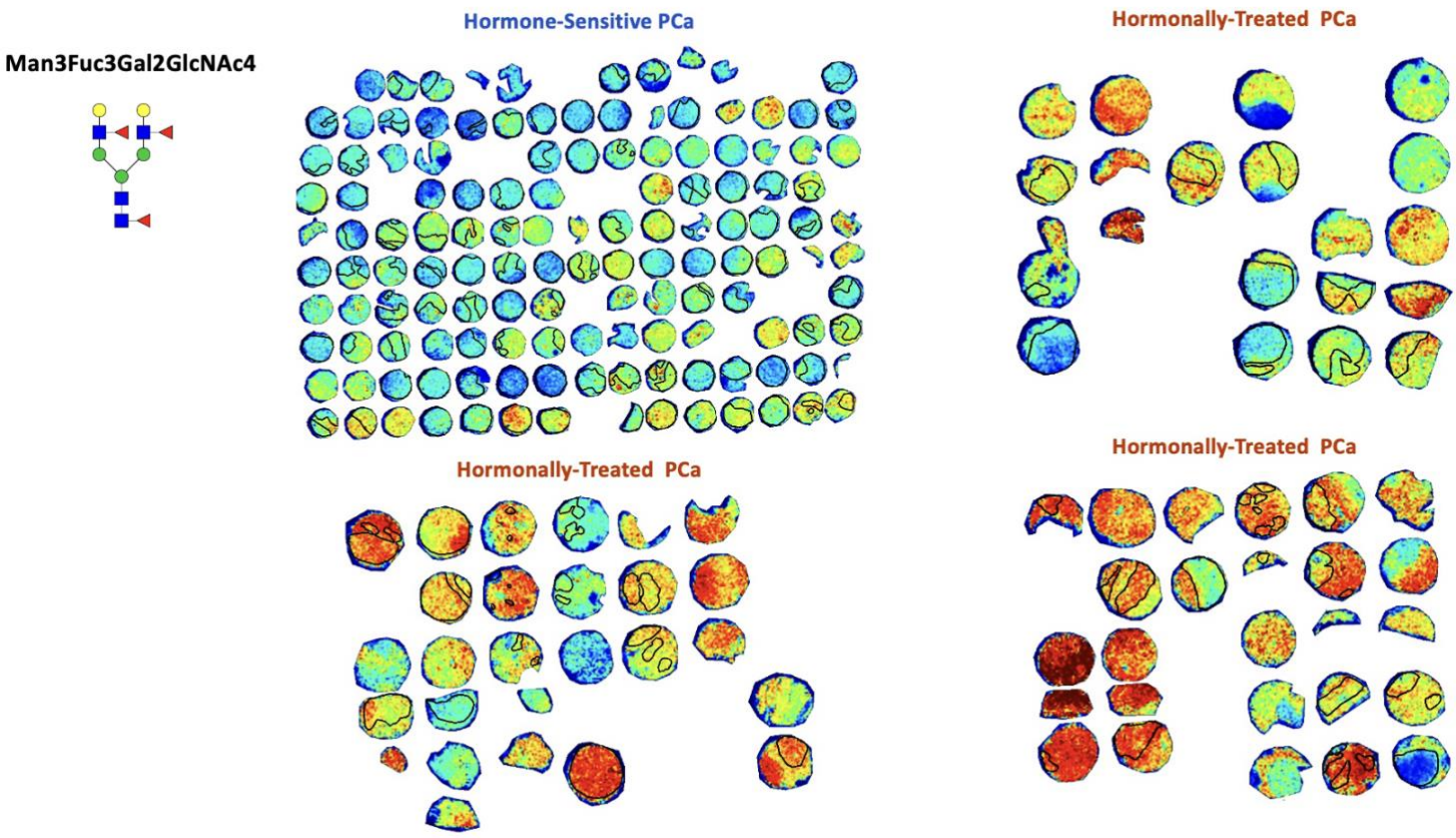


**Supplementary Figure 4: Representative glycan image demonstrating upregulation of a biantennary glycan (2101.7551 m/z) in hormonally-treated tumors (specific tumor regions demarcated in black).** Upregulated complex biantennary structures demonstrate localization both within demarcated tumor regions as well as in the surrounding stroma.

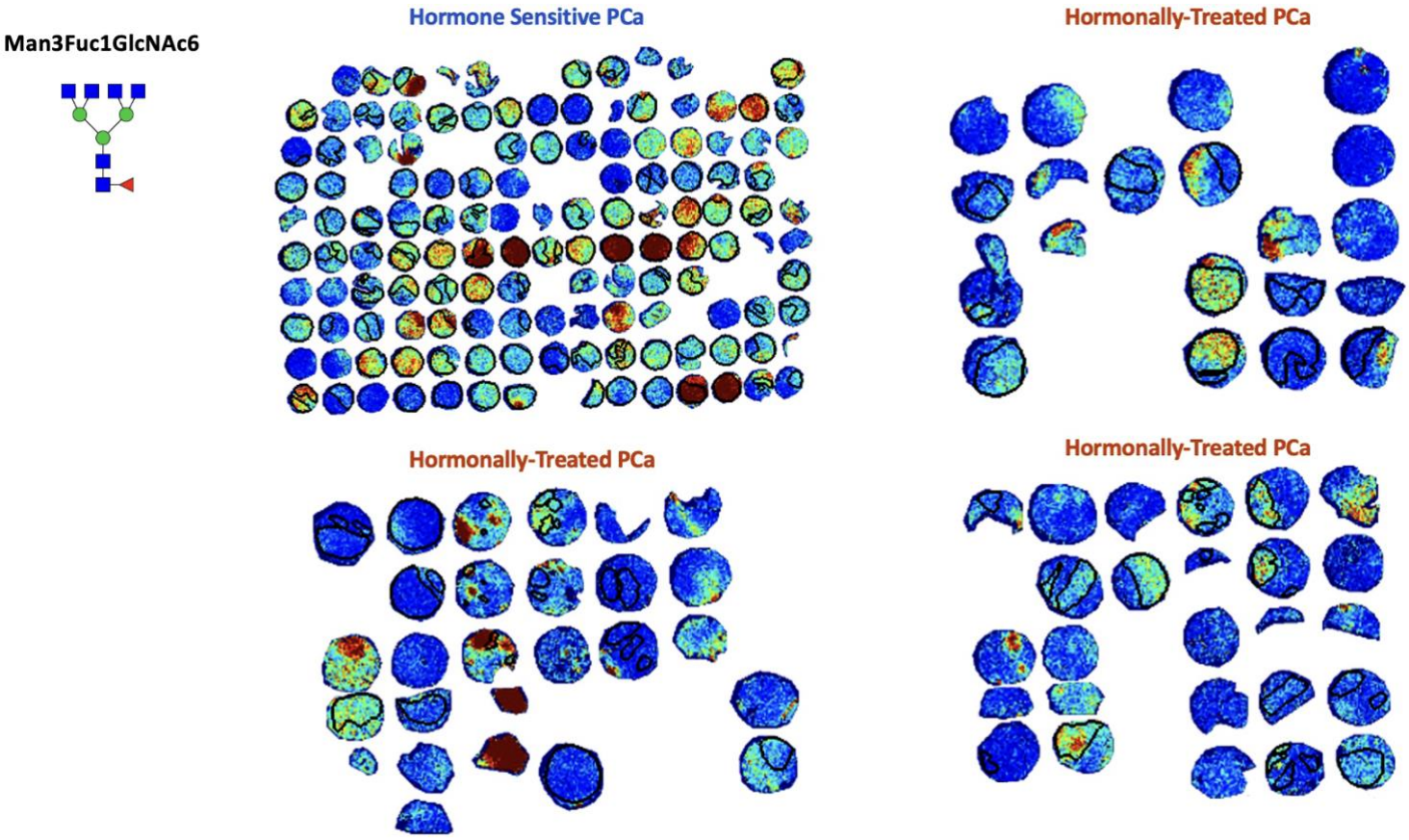


**Supplementary Figure 5: Representative glycan image demonstrating downregulation of a tetraantennary glycan (1891.6924 m/z) in hormonally-treated tumors (specific tumor regions demarcated in black).**

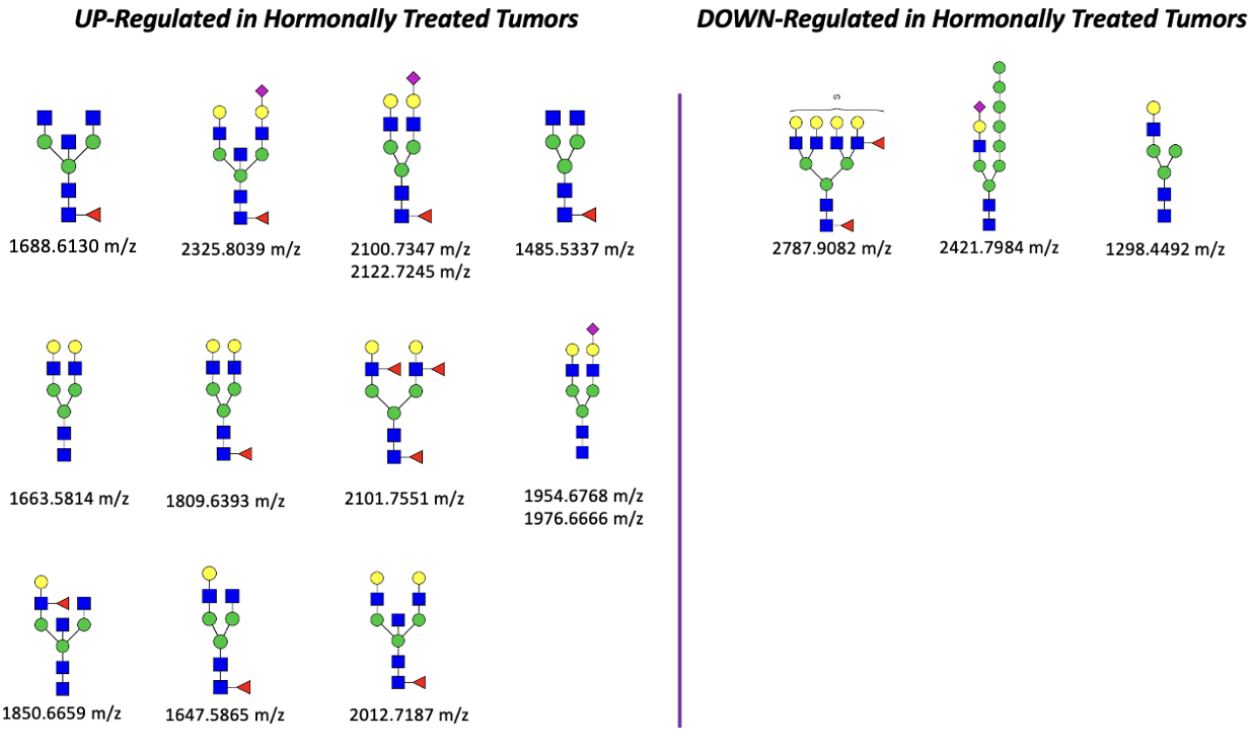


**Supplementary Figure 6. Significant *N*-glycans with a high degree of quantitative change in hormonally treated tumors.** These structure may serve as markers for PCa that is in remission and not yet resistant to androgen deprivation or AR inhibition.

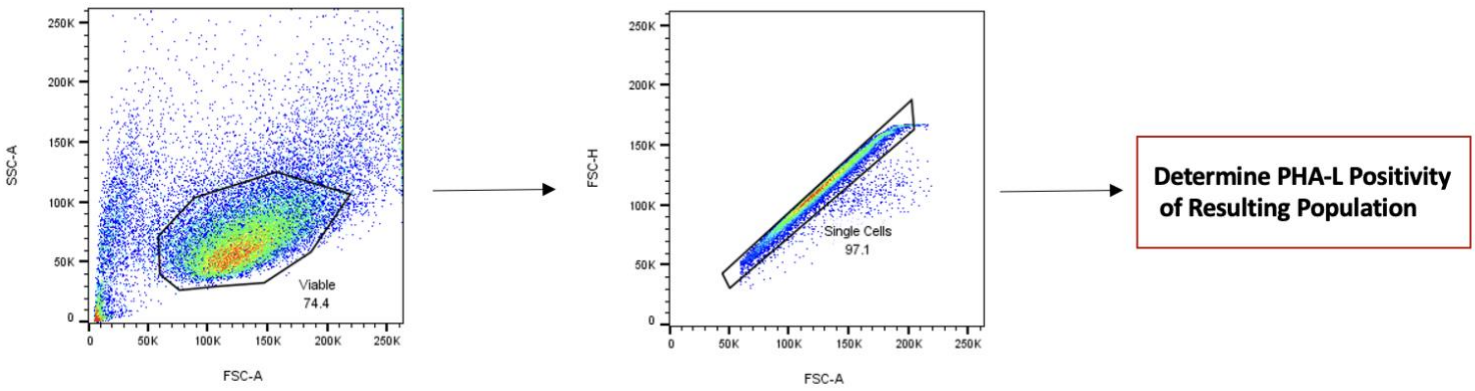


**Supplementary Figure 7: Gating Strategy for PHA-L Flow Cytometric Assays**

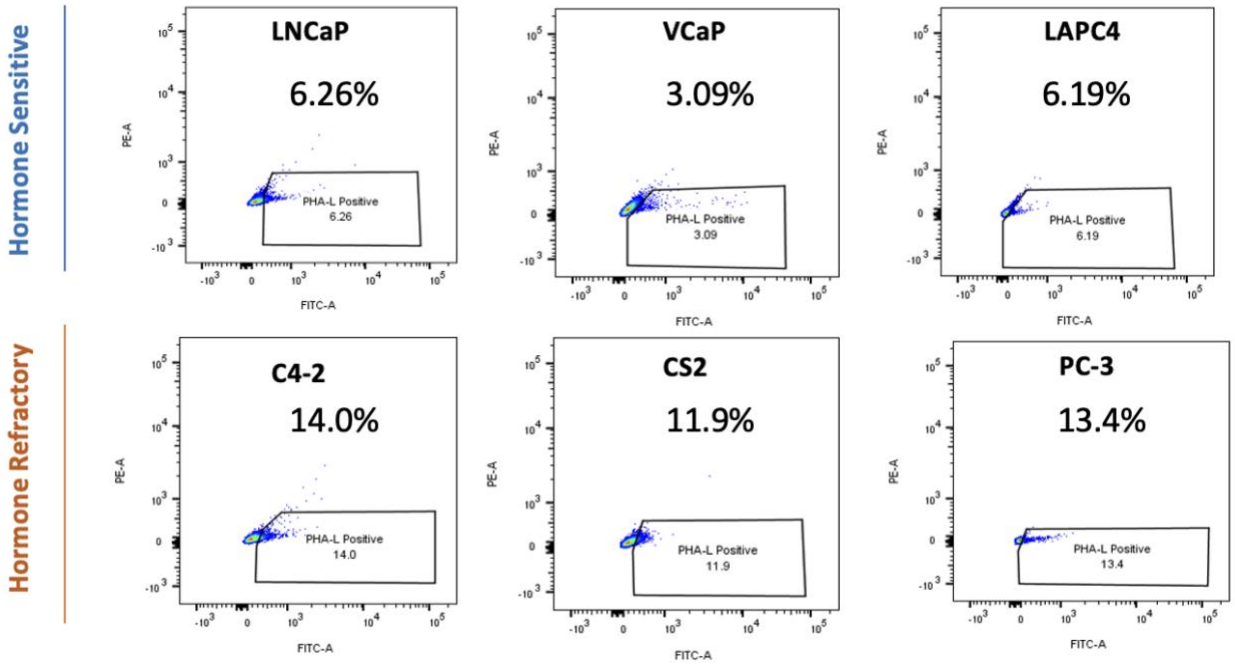


**Supplementary Figure 8: Flow cytometric analysis of hormone-sensitive cell lines and hormone-refractory cell lines for PHA-L reactivity.** PHA-L demonstrates the highest reactivity in hormone-refractory lines indicating these cells have a higher degree of β1-6 branched N-glycans on the cell surface.

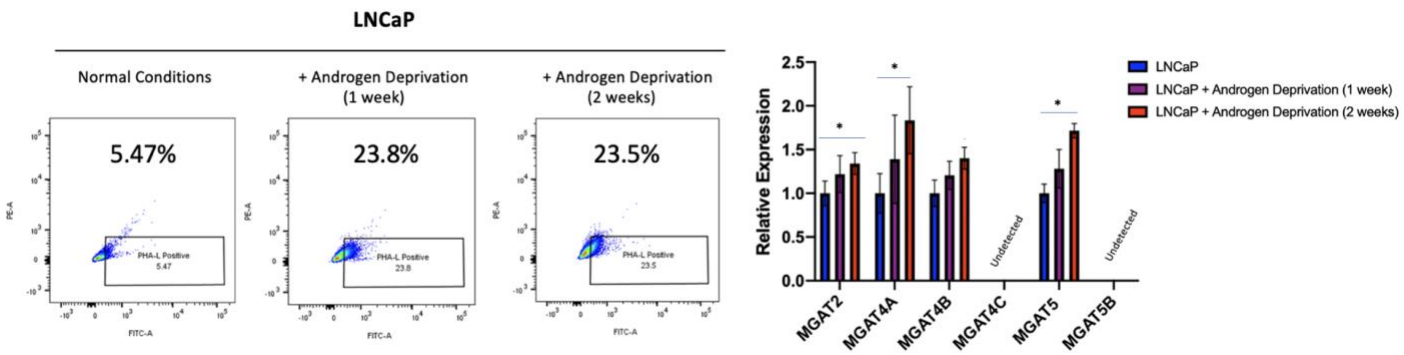


**Supplementary Figure 9: Flow cytometric analysis of LNCaP cells for PHA-L activity and RT-qPCR demonstrating expression level of N-glycan branching enzymes.** Androgen deprivation induces in vitro induces upregulation of branched N-glycans with elevated levels of MGAT2, MGAT4A, MGAT4B, and MGAT5. Two-way ANOVA was used for multiple comparisons with $p < 0.05$ considered significant. The following system was used to denote significance: $p < 0.05$ (*), $p < 0.01$ (**), $p < 0.0001$ (***), $p < 0.00001$ (****). Error bars correspond to standard deviation.

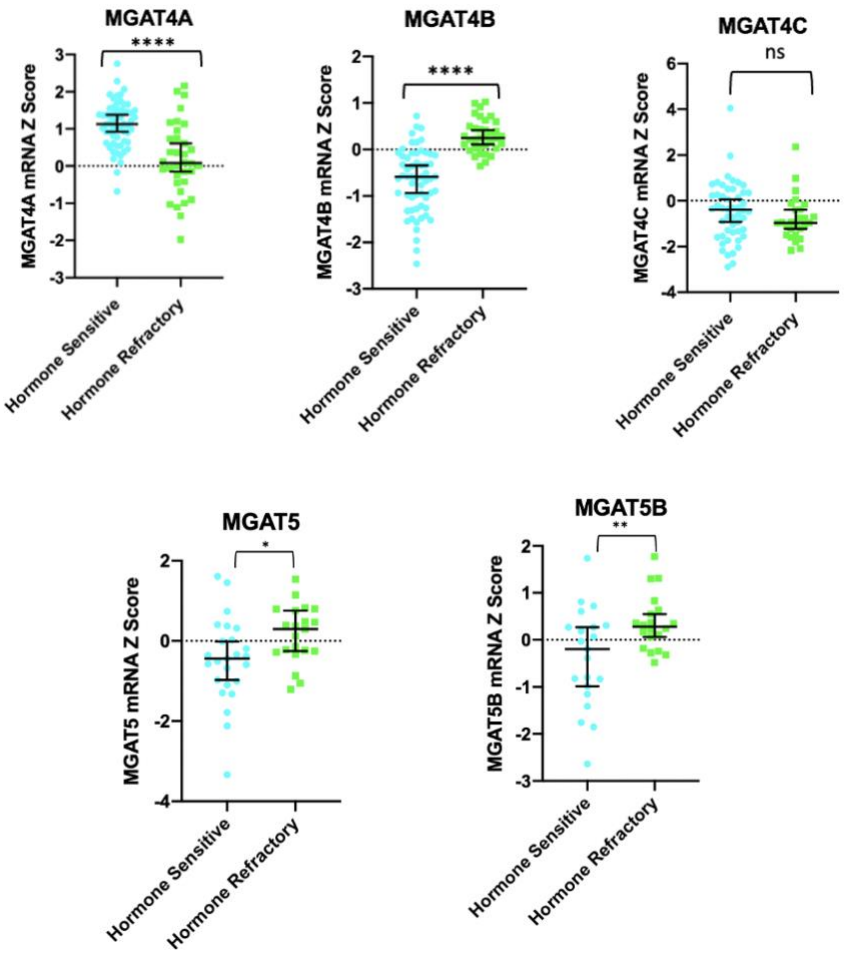


**Supplementary Figure 10: MGAT4 and MGAT5 mRNA levels in hormone refractory PCa patients.** MGAT4B, MGAT5, and MGAT5B demonstrate upregulated mRNA levels in hormone-refractory patients suggesting overall upregulated pathway activity. Statistics performed between each group by multiple, unpaired t test with $p < 0.05$ considered significant. The following system was used to denote significance: $p < 0.05$ (*), $p < 0.01$ (**), $p < 0.0001$ (***), $p < 0.00001$ (****). Error bars correspond to standard deviation.

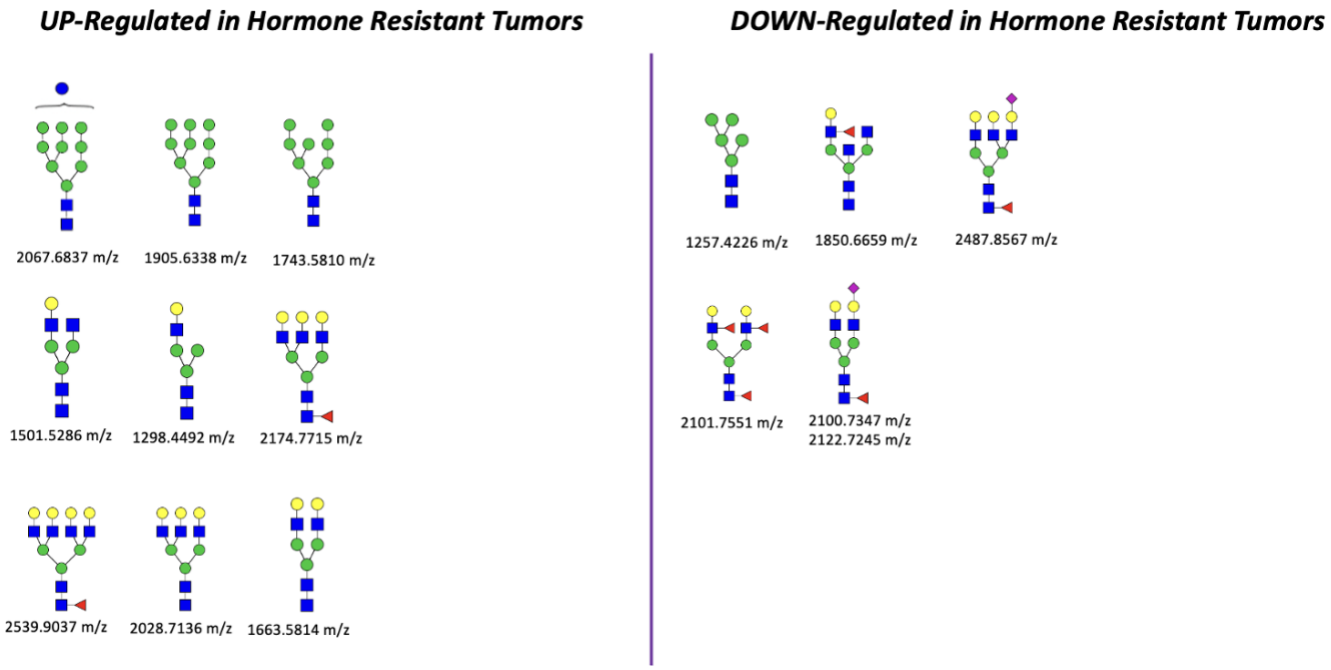


**Supplementary Figure 11. Significant *N*-glycans with a high degree of quantitative change in hormone resistant tumors.** These structures may serve as valuable markers for tumors that have developed resistance following hormonal therapy or be studied as potential therapeutic targets.

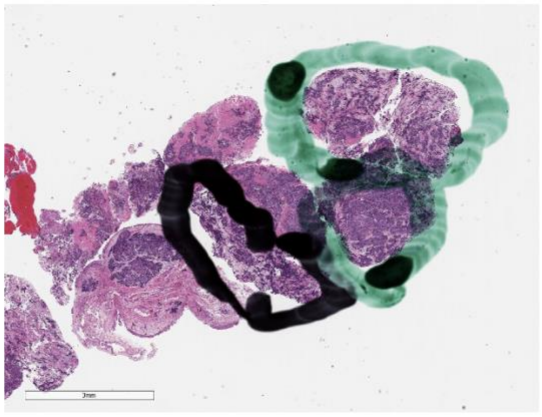

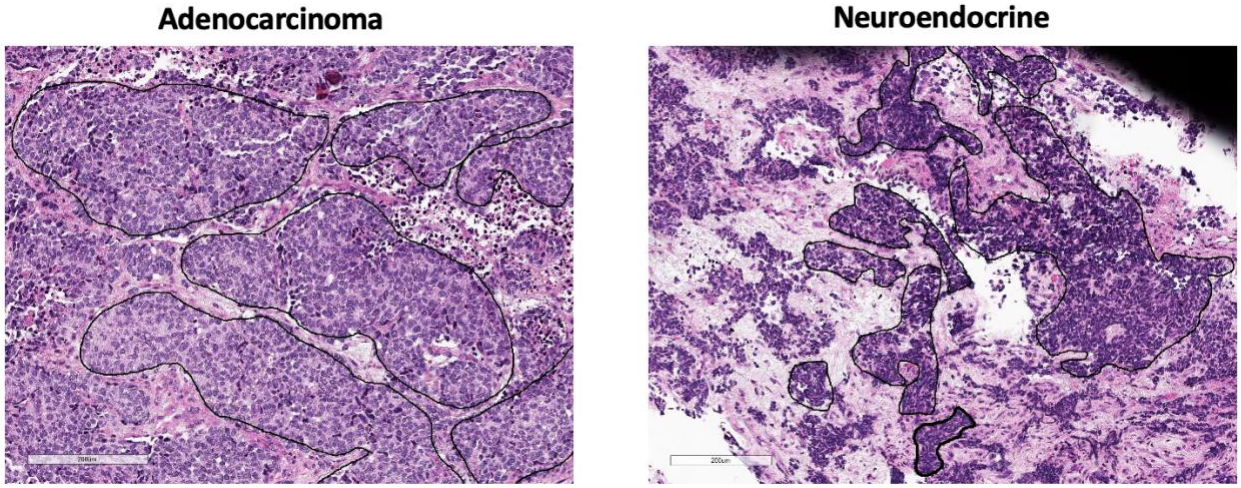


**Supplementary Figure 12: Representative H&E images of a patient case with both adenocarcinoma and neuroendocrine tumor cells on same FFPE slide. Upper panel demonstrates pathological annotation of targeted tumor regions (green = abundance of adenocarcinoma tumor cells, black = abundance of neuroendocrine tumor cells). Lower panel demonstrates representative demarcated (black circles) pure tumor cell regions within targeted areas.**

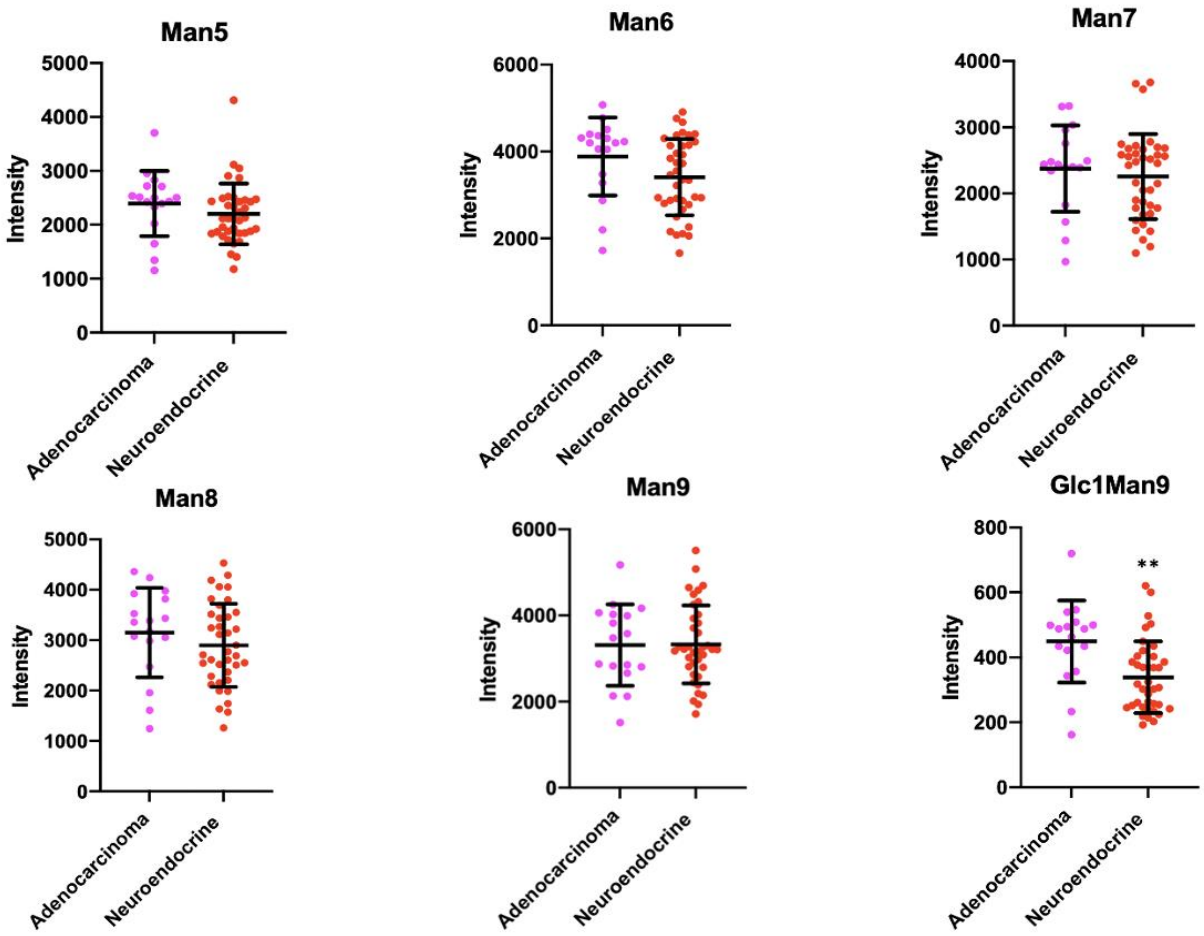


**Supplementary Figure 13: Scatter plots depicting high mannose (Man 5-9) structure abundance between all adenocarcinoma (n = 17) and NE regions (n = 38).** The levels of high mannose glycans remain relatively maintained between both regions with only Glc1Man9 demonstrating a small downregulation in NE tumor regions. Statistics performed between each group by multiple, unpaired t test with $p < 0.05$ considered significant. The following system was used to denote significance: $p < 0.05$ (*), $p < 0.01$ (**), $p < 0.0001$ (***), $p < 0.00001$ (****). Error bars correspond to standard deviation.

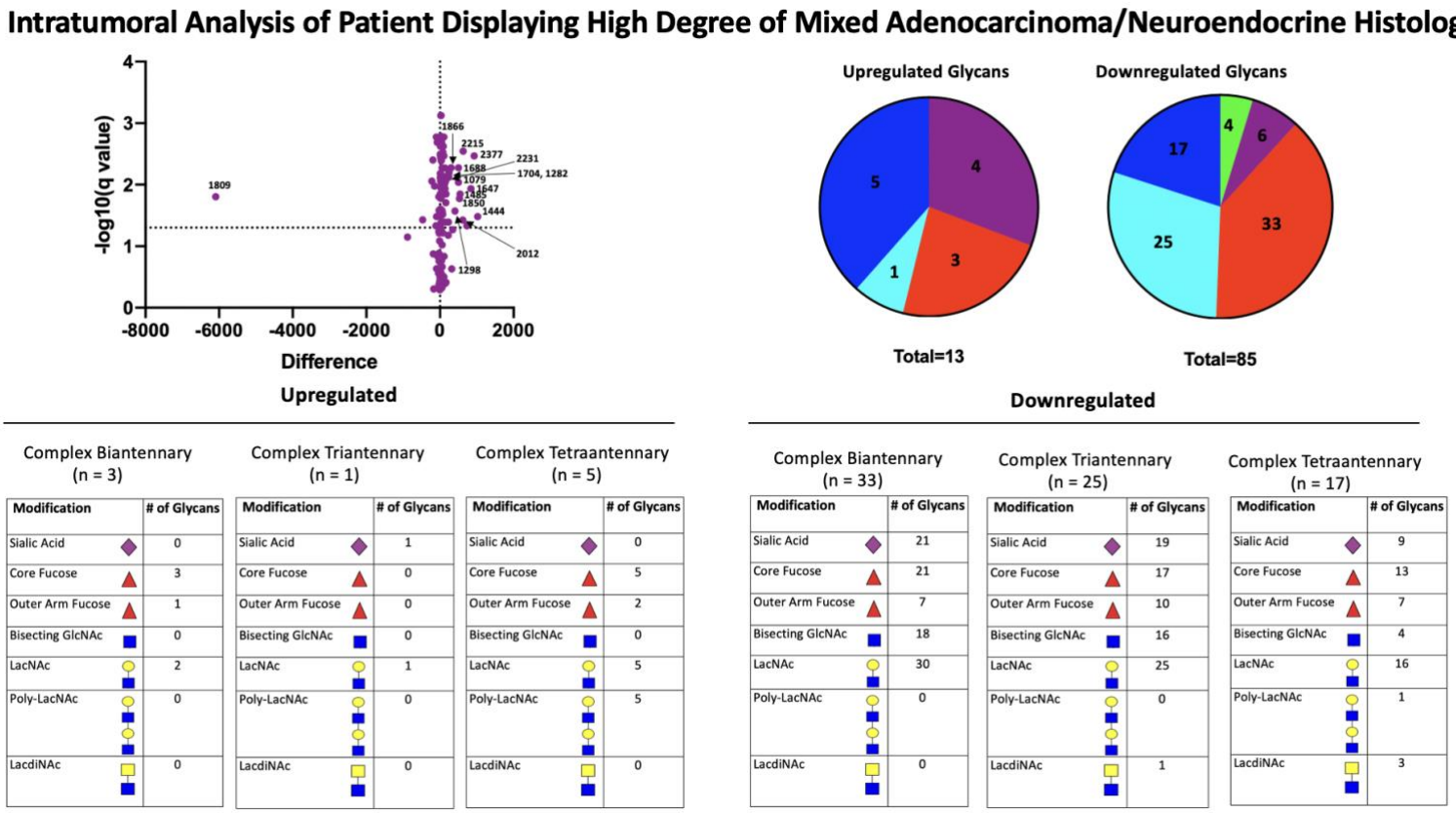


**Supplementary Figure 14: Analysis of N-glycosylation changes in patient with a high degree of mixed adenocarcinoma/neuroendocrine histology.** The vast majority of structures are downregulated and consist of complex-type glycans. Interestingly, in this patient, all upregulated tetraantennary glycans contained poly-LacNAc (a modification commonly associated with metastasis).

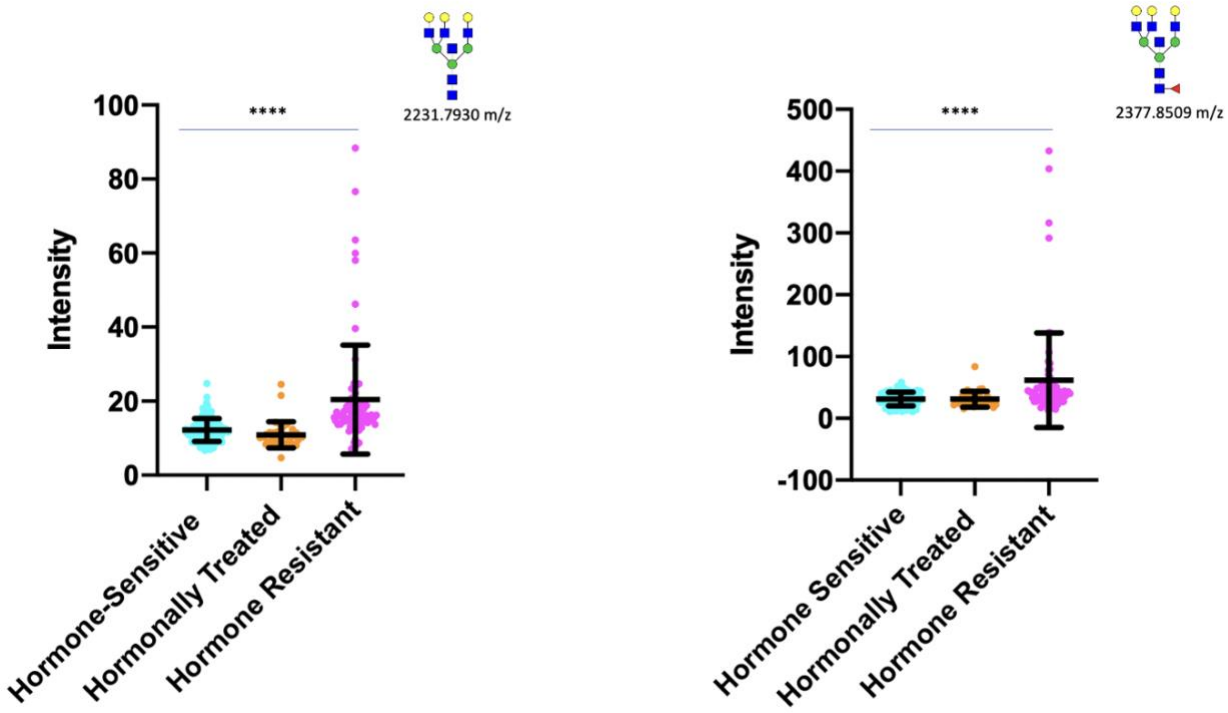


**Supplementary Figure 15: Scatter plots depicting non-fucosylated and fucosylated Gal3Man3GlcNAc6 levels in hormone-sensitive (n = 120), hormonally treated (n = 37), and hormone resistant (n = 75) tumor regions.** One-way ANOVA was used for multiple comparisons with $p < 0.05$ considered significant. The following system was used to denote significance: $p < 0.05$ (*), $p < 0.01$ (**), $p < 0.0001$ (***), $p < 0.00001$ (****). Error bars correspond to standard deviation.

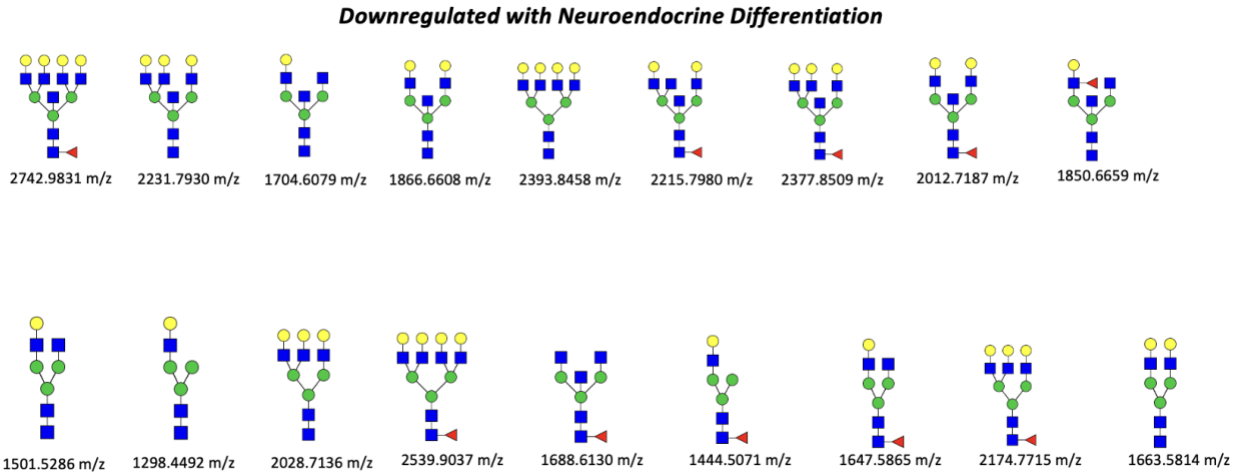


**Supplementary Figure 16: Significant N-glycans with a high degree of quantitative change in NE tumor regions.** These structures may serve as useful markers for determining whether tumors are undergoing NE differentiation.